AIAA JOURNAL
Vol. 48, No. 7, July 2010

Simulation of Sandia Flame D Using Velocity–Scalar Filtered Density Function

M. B. Nik,* S. L. Yilmaz,* and P. Givi†
University of Pittsburgh, Pittsburgh, Pennsylvania 15261
M. R. H. Sheikhi‡
Northeastern University, Boston, Massachusetts 02115
and
S. B. Pope§
Cornell University, Ithaca, New York 14853

DOI: 10.2514/1.J050154

The joint velocity–scalar filtered mass density function methodology is employed for large eddy simulation of Sandia National Laboratories' flame D. This is a turbulent piloted nonpremixed methane jet flame. In velocity–scalar filtered mass density function, the effects of the subgrid-scale chemical reaction and convection appear in closed forms. The modeled transport equation for the velocity–scalar filtered mass density function is solved by a hybrid finite difference/Monte Carlo scheme. For this flame, which exhibits little local extinction, a flamelet model is employed to relate the instantaneous composition to mixture fraction. The simulated results are assessed via comparison with laboratory data and show favorable agreements.

Nomenclature

a	=	flamelet strain rate, 1/s
C_0	=	model constant
C_ϵ	=	model constant
C_ϕ	=	model constant
c_{p_α}	=	constant pressure specific heat for species α, J/kg · K
D	=	nozzle diameter, m
G	=	filter function
h	=	enthalpy, J/kg
h_α^0	=	enthalpy of formation, J/kg
J_j^α	=	scalar flux for species α in j direction, kg/m^2 · s
k	=	subgrid kinetic energy, m^2/s^2
M_α	=	molecular weight of species α, kg/kmol
N_E	=	number of computational particles within an ensemble domain
N_s	=	number of species
Pr	=	Prandtl number
P_L	=	velocity–scalar filtered mass density function, kg
p	=	pressure, Pa
Q	=	transport variable
R	=	mixture gas constants, J/kg · K
Re	=	Reynolds number
R^0	=	universal gas constant, J/mol · K
r	=	radial coordinate, m
S_α	=	chemical reaction source terms, 1/s
Sc	=	Schmidt number
T	=	temperature, K
T_0	=	reference temperature, K
T'	=	integration dummy variable, K
t	=	time, s
U_{cl}	=	mean axial velocity at centerline, m/s
U_i^+	=	probabilistic representations of velocity vector, m/s
$\boldsymbol{u}$	=	Eulerian velocity, m/s
u_i	=	velocity vector, m/s
$\mathcal{V}_\mathcal{E}$	=	volume of ensemble domain, m^3
$\boldsymbol{v}$	=	sample space variable corresponding to velocity
W	=	Wiener process, s$^{\frac{1}{2}}$
X_i^+	=	probabilistic representations of position, m
x	=	Cartesian coordinate, m
$\mathbf{x}$	=	Cartesian coordinate, m
x'	=	integration dummy variable, m
Y	=	mass fraction
Y_α	=	species α mass fraction
y	=	Cartesian coordinate, m
z	=	Cartesian coordinate, m
Γ	=	mass molecular diffusivity coefficient, m^2/s
γ	=	thermal diffusivity coefficient, kg/m · s
Δ_L	=	large eddy simulation filter size, m
Δx	=	grid spacing in x direction, m
Δy	=	grid spacing in y direction, m
Δz	=	grid spacing in z direction, m
δ	=	Dirac delta function
ϵ	=	dissipation rate, m^2/s^3
ζ	=	fine-grained density
μ	=	absolute viscosity, kg/m · s
ρ	=	density, kg/m^3
τ_{ij}	=	viscous stress tensor, N/m^2
τ_L	=	subgrid-scale correlations
$\boldsymbol{\phi}$	=	composition vector
ϕ_α	=	scalar α
ϕ_α^+	=	probabilistic representations of scalar variables
$\boldsymbol{\psi}$	=	sample space variable corresponding to scalar
ω	=	subgrid-scale mixing frequency, 1/s

Received 25 August 2009; revision received 16 November 2009; accepted for publication 23 November 2009.

*Graduate Student, Mechanical Engineering and Material Science Department. Student Member AIAA.
†W. K. Whiteford Professor, Mechanical Engineering and Material Science Department. Associate Fellow AIAA.
‡Assistant Professor, Mechanical and Industrial Engineering. Senior Member AIAA.
§Sibley College Professor, Sibley School of Mechanical and Aerospace Engineering. Associate Fellow.

I. Introduction

THE filtered density function (FDF) [1–3] is now regarded as one of the most effective means of conducting large eddy simulation (LES) in turbulent combustion. In its initial form, the marginal scalar FDF (SFDF) [4] and its mass-weighted scalar filtered mass density function (SFMDF) [5] provided the first demonstration of a

transported FDF in reacting flows. The primary advantage of SFDF (SFMDF) is that it accounts for the subgrid-scale (SGS) chemical reaction in a closed form. This closure is one of the reasons for SFMDF's popularity and its widespread recent applications [6–27]. Inclusion of the velocity in the FDF accounts for the effects of convection in a closed form as well. This is demonstrated in the velocity-FDF [28], the joint velocity–scalar FDF [29] and its density-weighted velocity–scalar filtered mass density function (VSFMDF) [30] formulations. In its most rudimentary form, this methodology is equivalent to, at the least, a two-equation (second-order) SGS model. Note that the majority of conventional hydrodynamic SGS closures are algebraic (zero-order) [31].

Sheikhi et al. [30] demonstrate the predictive capability of the VSFMDF in capturing some of the intricate physics of SGS transport in nonreactive flows. Specifically, they show the advantages of this model over those in which the velocity–scalar correlation is modeled via a simplified gradient diffusion model. In the present work, the objective is to demonstrate the applicability of this improved methodology for prediction of reactive flows: specifically, hydrocarbon flames. For that, we consider the piloted nonpremixed methane jet flame as studied in the experiments of the Combustion Research Facility (CRF) at Sandia National Laboratories [32] and at the Technical University of Darmstadt [33]. This flame has been the subject of extensive previous LES via SFMDF by several investigators [12–14,19–24]. These contributions are ongoing; the CRF Web site[¶] maintains an updated bibliography of the growing literature in modeling of this flame. In the experiments, three flames are considered: flames D, E, and F. The geometrical configuration in these flames is the same, but the jet inlet velocity is varied. In flame D, the fuel jet velocity is the lowest. The jet velocity increases from flames D to E to F, with noticeable local extinctions in the latter two. To expand upon our previous SFMDF simulations [12], flame D is considered in this work. The objective is to assess the predictive capability of the VSFMDF in capturing the flowfield and the scalar mixing. This is the first application of the VSFMDF for prediction of a realistic hydrocarbon flame.

II. Formulation

A. Basic Equations

In a turbulent flow undergoing chemical reaction involving N_s species, the primary transport variables are the density $\rho(\mathbf{x}, t)$, the velocity vector $u_i(\mathbf{x}, t)$ $(i = 1, 2, 3)$, the pressure $p(\mathbf{x}, t)$, the enthalpy $h(\mathbf{x}, t)$, and the species' mass fractions $Y_\alpha(\mathbf{x}, t)$ $(\alpha = 1, 2, \ldots, N_s)$. The equations that govern the transport of these variables in space x_i $(i = 1, 2, 3)$ and time t are the continuity, momentum, enthalpy (energy), and species' mass-fraction equations, along with an equation of state:

$$\frac{\partial \rho}{\partial t} + \frac{\partial \rho u_j}{\partial x_j} = 0 \tag{1a}$$

$$\frac{\partial \rho u_i}{\partial t} + \frac{\partial \rho u_j u_i}{\partial x_j} = -\frac{\partial p}{\partial x_i} + \frac{\partial \tau_{ji}}{\partial x_j} \tag{1b}$$

$$\frac{\partial \rho \phi_\alpha}{\partial t} + \frac{\partial \rho u_j \phi_\alpha}{\partial x_j} = -\frac{\partial J_j^\alpha}{\partial x_j} + \rho S_\alpha, \qquad \alpha = 1, 2, \ldots, \sigma = N_s + 1 \tag{1c}$$

$$p = \rho R^0 T \sum_{\alpha=1}^{N_s} Y_\alpha / M_\alpha = \rho R T \tag{1d}$$

where R^0 and R are the universal and mixture gas constants, and M_α denotes the molecular weight of species α. The chemical reaction source terms $S_\alpha \equiv \hat{S}_\alpha(\boldsymbol{\phi}(\mathbf{x}, t))$ are functions of compositional scalars $(\boldsymbol{\phi} \equiv [\phi_1, \phi_2, \ldots, \phi_{N_s+1}])$. Equation (1c) represents the transport of species' mass fraction and enthalpy in a common form with

$$\phi_\alpha \equiv Y_\alpha, \qquad \alpha = 1, 2, \ldots, N_s,$$
$$\phi_\sigma \equiv h = \sum_{\alpha=1}^{N_s} h_\alpha \phi_\alpha, \qquad h_\alpha = h_\alpha^0 + \int_{T_0}^{T} c_{p_\alpha}(T')\, \mathrm{d}T' \tag{2}$$

where T and T_0 denote the temperature field and the reference temperature, respectively. In this equation, h_α^0 and c_{p_α} denote the enthalpy of formation at T_0 and the specific heat at constant pressure for species α. For a Newtonian fluid with Fick's law of diffusion, the viscous stress tensor τ_{ij} and the scalar flux J_j^α are represented by

$$\tau_{ij} = \mu\left(\frac{\partial u_i}{\partial x_j} + \frac{\partial u_j}{\partial x_i} - \frac{2}{3}\frac{\partial u_k}{\partial x_k}\delta_{ij}\right), \qquad J_j^\alpha = -\gamma \frac{\partial \phi_\alpha}{\partial x_j} \tag{3}$$

where μ is the fluid dynamic viscosity, and $\gamma = \rho\Gamma$ denotes the thermal and mass molecular diffusivity coefficients for all the scalars. We assume $\mu = \gamma$: i.e., unity Schmidt Sc and Prandtl Pr numbers. The viscosity and molecular diffusivity coefficients can, in general, be temperature-dependent; here, they are assumed to be constant.

B. Filtered Equations

Large eddy simulation involves the spatial filtering operation [31,34]:

$$\langle Q(\mathbf{x}, t)\rangle_\ell = \int_{-\infty}^{+\infty} Q(\mathbf{x}', t) G(\mathbf{x}', \mathbf{x})\, \mathrm{d}\mathbf{x}' \tag{4}$$

where $G(\mathbf{x}', \mathbf{x})$ denotes a filter function, and $\langle Q(\mathbf{x}, t)\rangle_\ell$ is the filtered value of the transport variable $Q(\mathbf{x}, t)$. In variable-density flows it is convenient to use the Favre-filtered quantity $\langle Q(\mathbf{x}, t)\rangle_L = \langle \rho Q\rangle_\ell / \langle \rho\rangle_\ell$. We consider a filter function that is spatially and temporally invariant and localized: thus, $G(\mathbf{x}', \mathbf{x}) \equiv G(\mathbf{x}' - \mathbf{x})$ with the properties $G(\mathbf{x}) \geq 0$ and

$$\int_{-\infty}^{+\infty} G(\mathbf{x})\, \mathrm{d}\mathbf{x} = 1$$

Applying the filtering operation to Eqs. (1) and using the conventional LES approximation for the diffusion terms, we obtain

$$\frac{\partial \langle \rho\rangle_\ell}{\partial t} + \frac{\partial \langle \rho\rangle_\ell \langle u_j\rangle_L}{\partial x_j} = 0 \tag{5a}$$

$$\begin{aligned}\frac{\partial \langle \rho\rangle_\ell \langle u_i\rangle_L}{\partial t} &+ \frac{\partial \langle \rho\rangle_\ell \langle u_j\rangle_L \langle u_i\rangle_L}{\partial x_j} \\ &= -\frac{\partial \langle p\rangle_\ell}{\partial x_i} + \frac{\partial}{\partial x_j}\left(\gamma\left(\frac{\partial \langle u_i\rangle_L}{\partial x_j} + \frac{\partial \langle u_j\rangle_L}{\partial x_i}\right)\right) \\ &\quad - \frac{2}{3}\frac{\partial}{\partial x_i}\left(\gamma \frac{\partial \langle u_j\rangle_L}{\partial x_j}\right) - \frac{\partial \langle \rho\rangle_\ell \tau_L(u_i, u_j)}{\partial x_j}\end{aligned} \tag{5b}$$

$$\begin{aligned}\frac{\partial \langle \rho\rangle_\ell \langle \phi_\alpha\rangle_L}{\partial t} &+ \frac{\partial \langle \rho\rangle_\ell \langle u_j\rangle_L \langle \phi_\alpha\rangle_L}{\partial x_j} \\ &= \frac{\partial}{\partial x_j}\left(\gamma \frac{\partial \langle \phi_\alpha\rangle_L}{\partial x_j}\right) - \frac{\partial \langle \rho\rangle_\ell \tau_L(u_j, \phi_\alpha)}{\partial x_j} + [\langle \rho\rangle_\ell \langle S_\alpha\rangle_L]\end{aligned} \tag{5c}$$

where τ_L denotes the SGS correlation: $\tau_L(a, b) = \langle ab\rangle_L - \langle a\rangle_L \langle b\rangle_L$.

C. Exact VSFMDF Transport Equation

The velocity–scalar filtered mass density function, denoted by P_L, is formally defined as [1]

[¶]Data available online at www.sandia.gov/TNF/biblio.html [retrieved 8 March 2010].

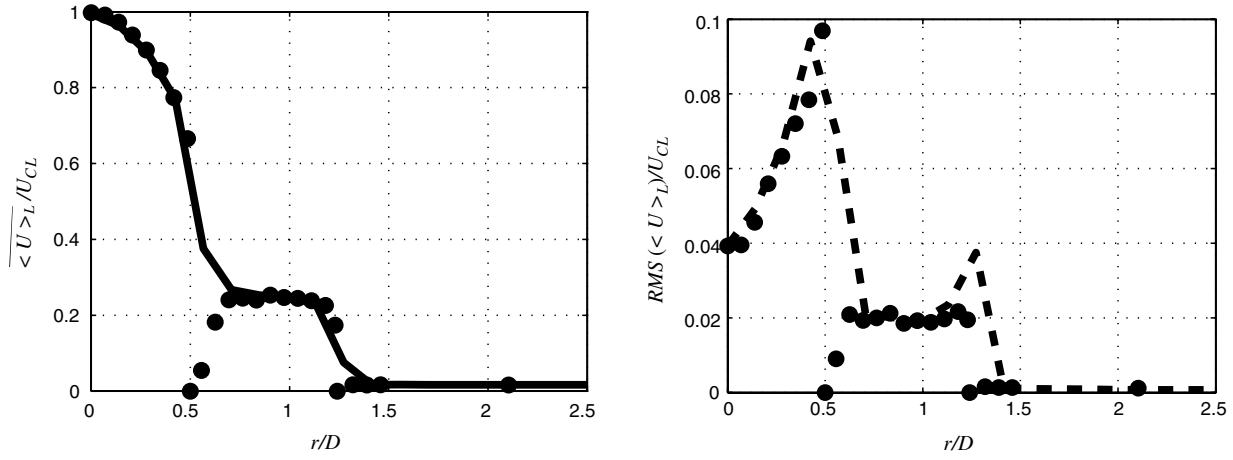

a) b)

Fig. 1 Radial distribution of the mean and rms values of the streamwise filtered velocity at $x/D = 0.138$. U_{cl} denotes the mean axial velocity at the centerline, the symbols denote the experimental data. The line denotes the mean value and the thick dashed line denotes the rms value: a) mean axial velocity and b) rms value of the axial velocity.

$$P_L(\boldsymbol{v}, \boldsymbol{\psi}, \mathbf{x}; t) = \int_{-\infty}^{+\infty} \rho(\mathbf{x}', t)\zeta(\boldsymbol{v}, \boldsymbol{\psi}; \boldsymbol{u}(\mathbf{x}', t), \boldsymbol{\phi}(\mathbf{x}', t))G(\mathbf{x}' - \mathbf{x})\,\mathrm{d}\mathbf{x}' \tag{6}$$

where

$$\zeta(\boldsymbol{v}, \boldsymbol{\psi}; \boldsymbol{u}(\mathbf{x}, t), \boldsymbol{\phi}(\mathbf{x}, t)) = \prod_{i=1}^{3} \delta(v_i - u_i(\mathbf{x}, t)) \times \prod_{\alpha=1}^{\sigma} \delta(\psi_\alpha - \phi_\alpha(\mathbf{x}, t)) \tag{7}$$

In Eqs. (6) and (7), δ denotes the Dirac delta function, and $\boldsymbol{v}$ and $\boldsymbol{\psi}$ are the velocity vector and the scalar array in the sample space. The term ζ is the fine-grained density [35,36]. Equation (6) defines the VSFMDF as the spatially filtered value of the fine-grained density. With the condition of a positive filter kernel [37], P_L has all of the properties of a mass density function [36]. Considering the time derivative of the fine-grained density function [Eq. (7)] and using Eqs. (1b), (1c), (3), and (6) results in

$$\frac{\partial P_L}{\partial t} + \frac{\partial v_j P_L}{\partial x_j} = \frac{\partial}{\partial v_i}\left(\left\langle \frac{1}{\rho(\boldsymbol{\phi})}\frac{\partial p}{\partial x_i}\middle| \boldsymbol{v}, \boldsymbol{\psi}\right\rangle_\ell P_L\right) - \frac{\partial}{\partial v_i}\left(\left\langle \frac{1}{\rho(\boldsymbol{\phi})}\frac{\partial \tau_{ji}}{\partial x_j}\middle| \boldsymbol{v}, \boldsymbol{\psi}\right\rangle_\ell P_L\right) + \frac{\partial}{\partial \psi_\alpha}\left(\left\langle \frac{1}{\rho(\boldsymbol{\phi})}\frac{\partial J_i^\alpha}{\partial x_i}\middle| \boldsymbol{v}, \boldsymbol{\psi}\right\rangle_\ell P_L\right) - \frac{\partial}{\partial \psi_\alpha}(S_\alpha(\boldsymbol{\psi})P_L)$$

This is an exact transport equation and indicates that the effects of convection (the second term on left-hand side) and chemical reaction (the last term on the right-hand side) appear in closed forms. The unclosed terms denote convective effects in the velocity–scalar sample space. These terms are exhibited by the conditional filtered [30] values, as shown by the first three terms on the right-hand side.

D. Modeled VSFMDF Transport Equation

For closure of the VSFMDF transport equation, we consider the general diffusion process [38], given by the system of stochastic differential equations. In this context, developed in [4,28,29,39,40], we use the simplified Langevin model and the linear mean-square-estimation model [35]:

$$\mathrm{d}X_i^+ = U_i^+\,\mathrm{d}t + \sqrt{\frac{2\gamma}{\langle\rho\rangle_\ell}}\mathrm{d}W_i \tag{8a}$$

$$\mathrm{d}U_i^+ = \left[-\frac{1}{\langle\rho\rangle_\ell}\frac{\partial\langle p\rangle_\ell}{\partial x_i} + \frac{2}{\langle\rho\rangle_\ell}\frac{\partial}{\partial x_j}\left(\gamma\frac{\partial\langle u_i\rangle_L}{\partial x_j}\right) + \frac{1}{\langle\rho\rangle_\ell}\frac{\partial}{\partial x_j}\left(\gamma\frac{\partial\langle u_j\rangle_L}{\partial x_i}\right) - \frac{2}{3}\frac{1}{\langle\rho\rangle_\ell}\frac{\partial}{\partial x_i}\left(\gamma\frac{\partial\langle u_j\rangle_L}{\partial x_j}\right)\right]\mathrm{d}t + G_{ij}(U_j^+ - \langle u_j\rangle_L)\,\mathrm{d}t + \sqrt{C_0\epsilon}\,\mathrm{d}W_i' + \sqrt{\frac{2\gamma}{\langle\rho\rangle_\ell}}\frac{\partial\langle u_i\rangle_L}{\partial x_j}\,\mathrm{d}W_j \tag{8b}$$

$$\mathrm{d}\,\phi_\alpha^+ = -C_\phi\omega(\phi_\alpha^+ - \langle\phi_\alpha\rangle_L)\,\mathrm{d}t + S_\alpha(\boldsymbol{\phi})\,\mathrm{d}t \tag{8c}$$

where

$$G_{ij} = -\omega\left(\frac{1}{2} + \frac{3}{4}C_0\right)\delta_{ij}, \qquad \omega = \frac{\epsilon}{k}$$
$$\epsilon = C_\epsilon\frac{k^{3/2}}{\Delta_L}, \qquad k = \frac{1}{2}\tau_L(u_i, u_i) \tag{9}$$

X_i^+ and U_i^+, ϕ_α^+ are probabilistic representations of position, velocity vector, and scalar variables, respectively. W terms denote the Wiener–Lévy processes [41,42]. In Eq. (9), ω is the SGS mixing

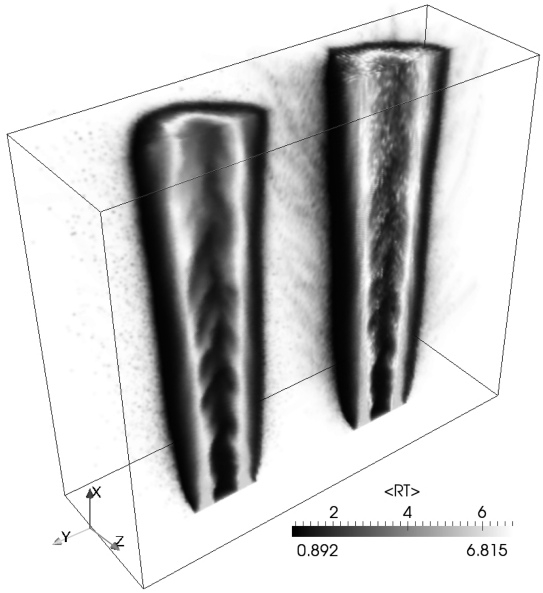

Fig. 2 Instantaneous filtered *RT* fields (normalized by the freestream values) as obtained via MC (left) and FD (right).

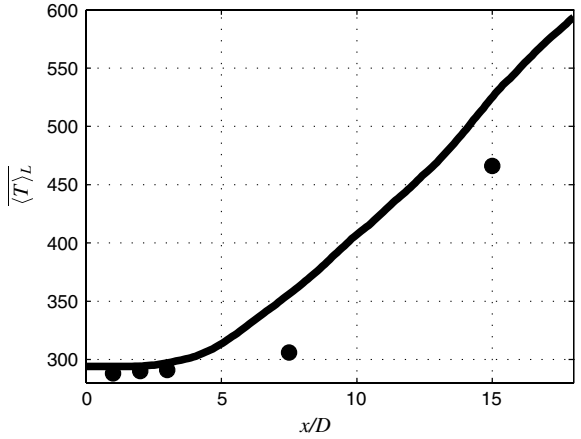

Fig. 3 Axial distribution of the mean filtered temperature at $r/D = 0$. The symbols denote the experimental data and the solid line denotes the predicted values.

frequency, ϵ is the dissipation rate, k is the SGS kinetic energy, and Δ_L is the LES filter size. The model parameters are the same as those suggested by Sheikhi et al. [30]: $C_0 = 2.1$, $C_\phi = 1.0$, and $C_\epsilon = 1.0$. No attempt is made to optimize the values of these parameters.

E. Numerical Solution

Numerical solution of the modeled VSFMDF transport equation is obtained by a hybrid finite difference (FD) and Monte Carlo (MC) procedure. The computational domain is discretized on equally spaced finite difference grid points and the FMDF is represented by an ensemble of statistically identical MC particles that carry information pertaining to the velocity and the scalar values. This information is updated via temporal integration of the stochastic differential equations. Statistical information is obtained by considering an ensemble of N_E computational particles residing within an ensemble domain of volume $\mathcal{V}_E$ centered around each of the FD grid points. To reduce the computational cost, a procedure involving the use of nonuniform weights is also considered. This procedure allows a smaller number of particles in regions where a low degree of variability is expected. Conversely, in regions of high variability, a large number of particles is allowed. The sum of weights within the ensemble domain is related to filtered fluid density [43].

The FD solver is fourth-order-accurate in space and second-order-accurate in time [44]. All of the FD operations are conducted on fixed grid points. The transfer of information from the FD points to the MC particles is accomplished via a linear interpolation. The inverse transfer is accomplished via ensemble-averaging. The FD transport equations include unclosed second-order moments that are obtained from the MC. Further details on the hybrid FD-MC can be found in [43].

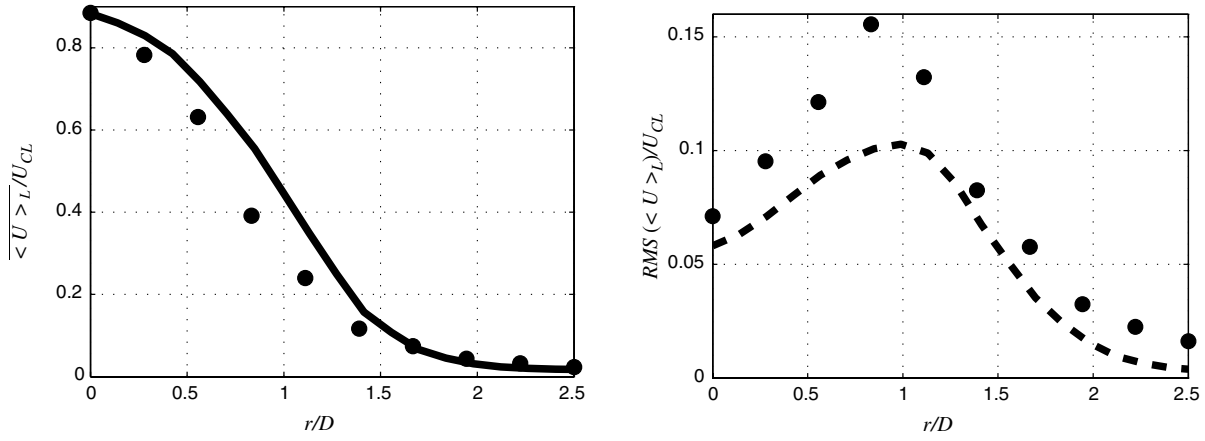

a) b)

Fig. 4 Radial distribution of the mean and rms values of the filtered axial velocity. U_{cl} denotes the mean axial velocity at the centerline at the inlet, the symbols denote the experimental data. The line denotes the mean value and the thick dashed line denotes the rms value: a) mean axial velocity at $x/D = 15$and b) rms value of the axial velocity at $x/D = 15$.

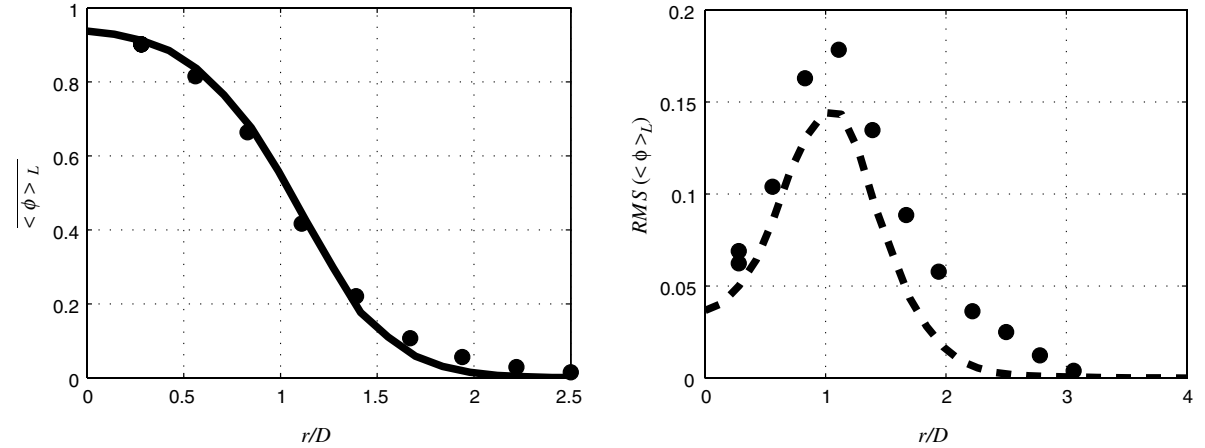

a) b)

Fig. 5 Radial distribution of the mean and rms values of the filtered mixture fraction. The symbols denote the experimental data. The line denotes the mean value and the thick dashed line denotes the rms value: a) mean mixture fraction at $x/D = 15$and b) rms value of the mixture fraction at $x/D = 15$.

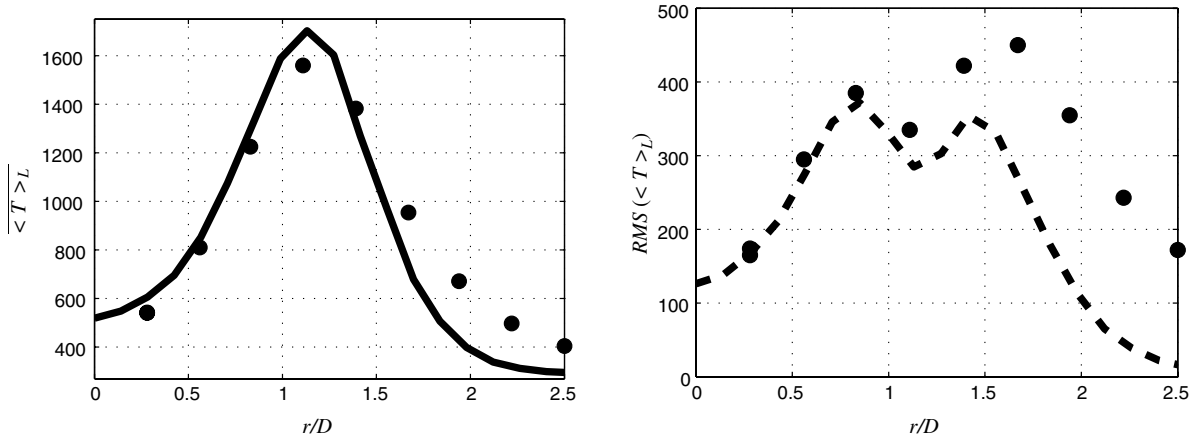

a) b)

Fig. 6 Radial distribution of the mean and rms values of the filtered temperature values. The symbols denote the experimental data. The line denotes the mean value and the thick dashed line denotes the rms value: a) mean temperature (K) at $x/D = 15$and b) rms value of the temperature (K) at $x/D = 15$.

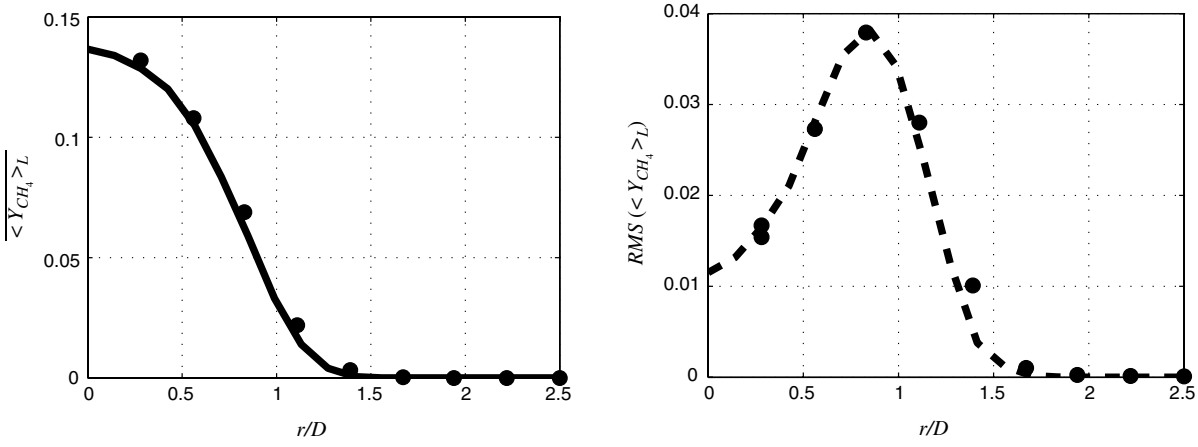

a) b)

Fig. 7 Radial distribution of the mean and rms values of filtered CH_4 mass fractions. The symbols denote the experimental data. The line denotes the mean value and the thick dashed line denotes the rms value: a) mean CH_4 mass fraction at $x/D = 15$and b) rms value of CH_4 mass fraction at $x/D = 15$.

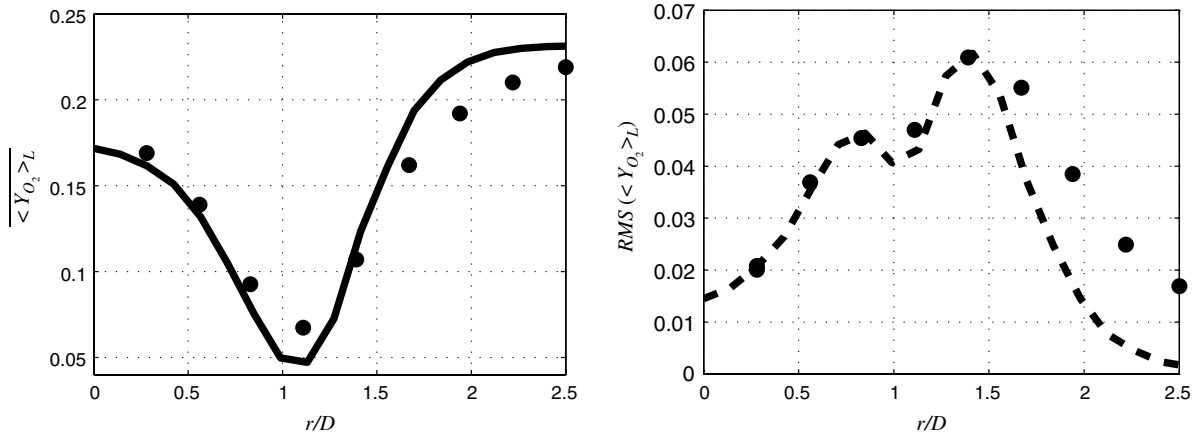

a) b)

Fig. 8 Radial distribution of the mean and rms values of the filtered O_2 mass fractions. The symbols denote the experimental data. The line denotes the mean value and the thick dashed line denotes the rms value: a) mean O_2 mass fraction at $x/D = 15$and b) rms value of O_2 mass fraction at $x/D = 15$.

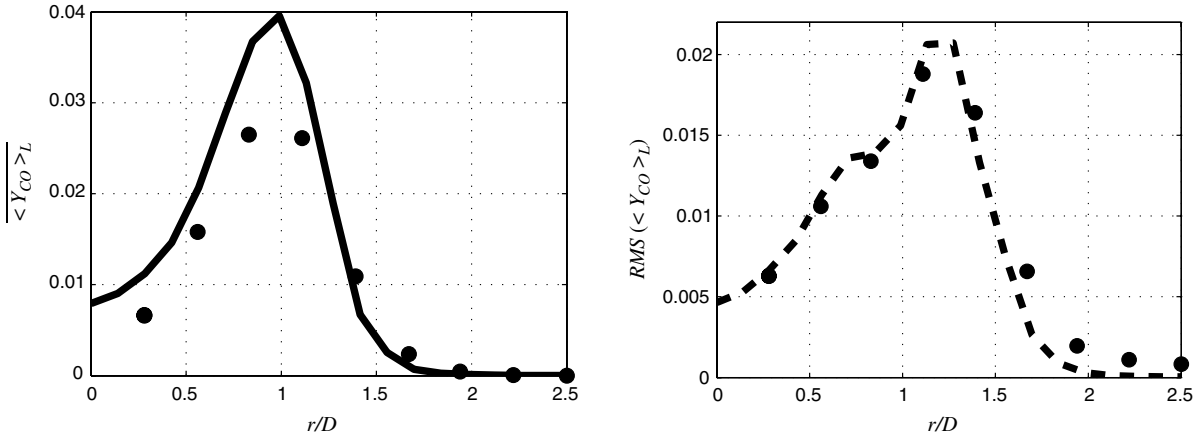

a) b)

Fig. 9 Radial distribution of the mean and rms values of the filtered CO mass fractions. The symbols denote experimental data. The line denotes the mean value and the thick dashed line denotes the rms value: a) mean CO mass fraction at $x/D = 15$and b) rms value of CO mass fraction at $x/D = 15$.

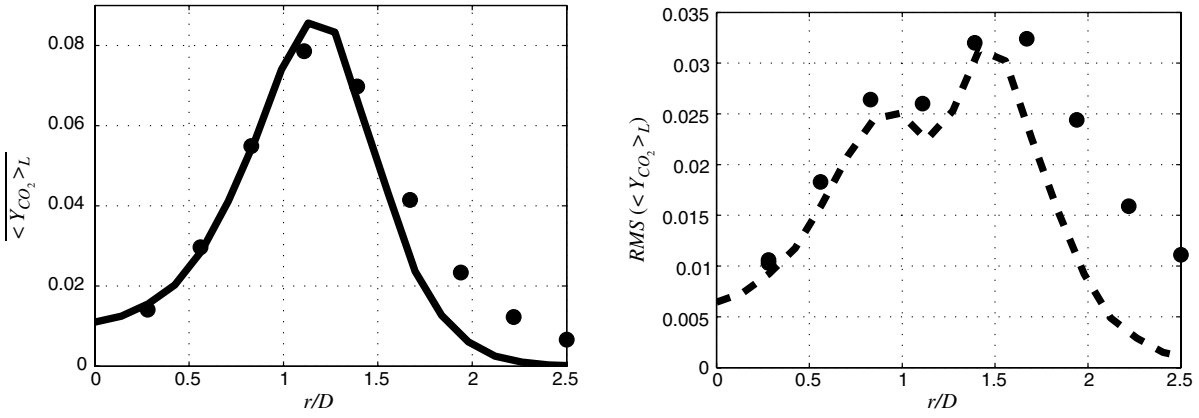

a) b)

Fig. 10 Radial distribution of the mean and rms values of the filtered CO_2 mass fractions. The symbols denote the experimental data. The line denotes the mean value and the thick dashed line denotes the rms value: a) mean CO_2 mass fraction at $x/D = 15$and b) rms value of CO_2 mass fraction at $x/D = 15$.

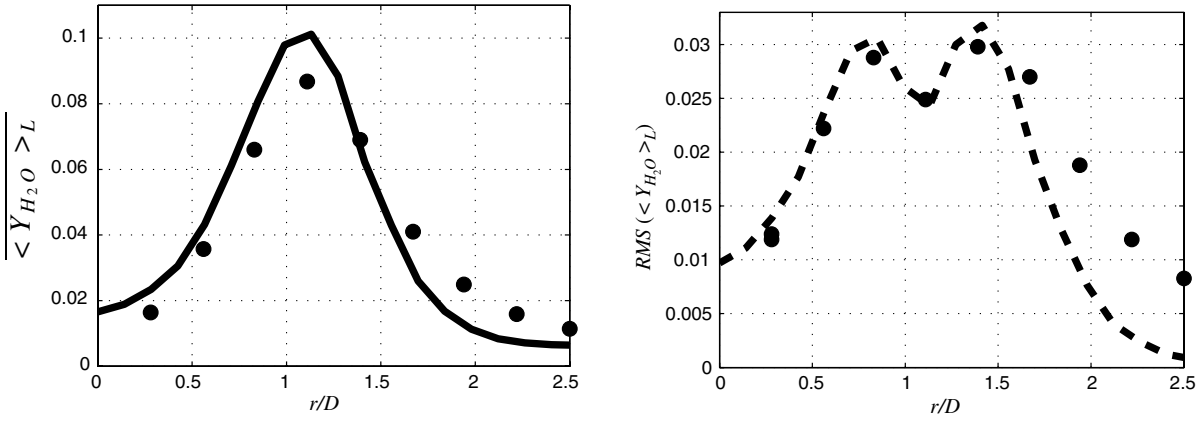

a) b)

Fig. 11 Radial distribution of the mean and rms values of the filtered H_2O mass fractions. The symbols denote the experimental data. The line denotes the mean value and the thick dashed line denotes the rms value: a) mean H_2O mass fraction at $x/D = 15$and b) rms value of H_2O mass fraction at $x/D = 15$.

III. Flow Configuration and Simulation Parameters

Sandia flame D consists of a main jet with a mixture of 25% methane and 75% air by volume. The nozzle is placed in a coflow of air and the flame is stabilized by a substantial pilot. The Reynolds number for the main jet is $Re = 22,400$ based on the nozzle diameter $D = 7.2$ mm and the bulk jet velocity 49.6 m/s.

Simulations are conducted on a three-dimensional Cartesian mesh with uniform spacings in each of the three directions. With available resources, simulations are afforded within a domain spanning $18D \times$

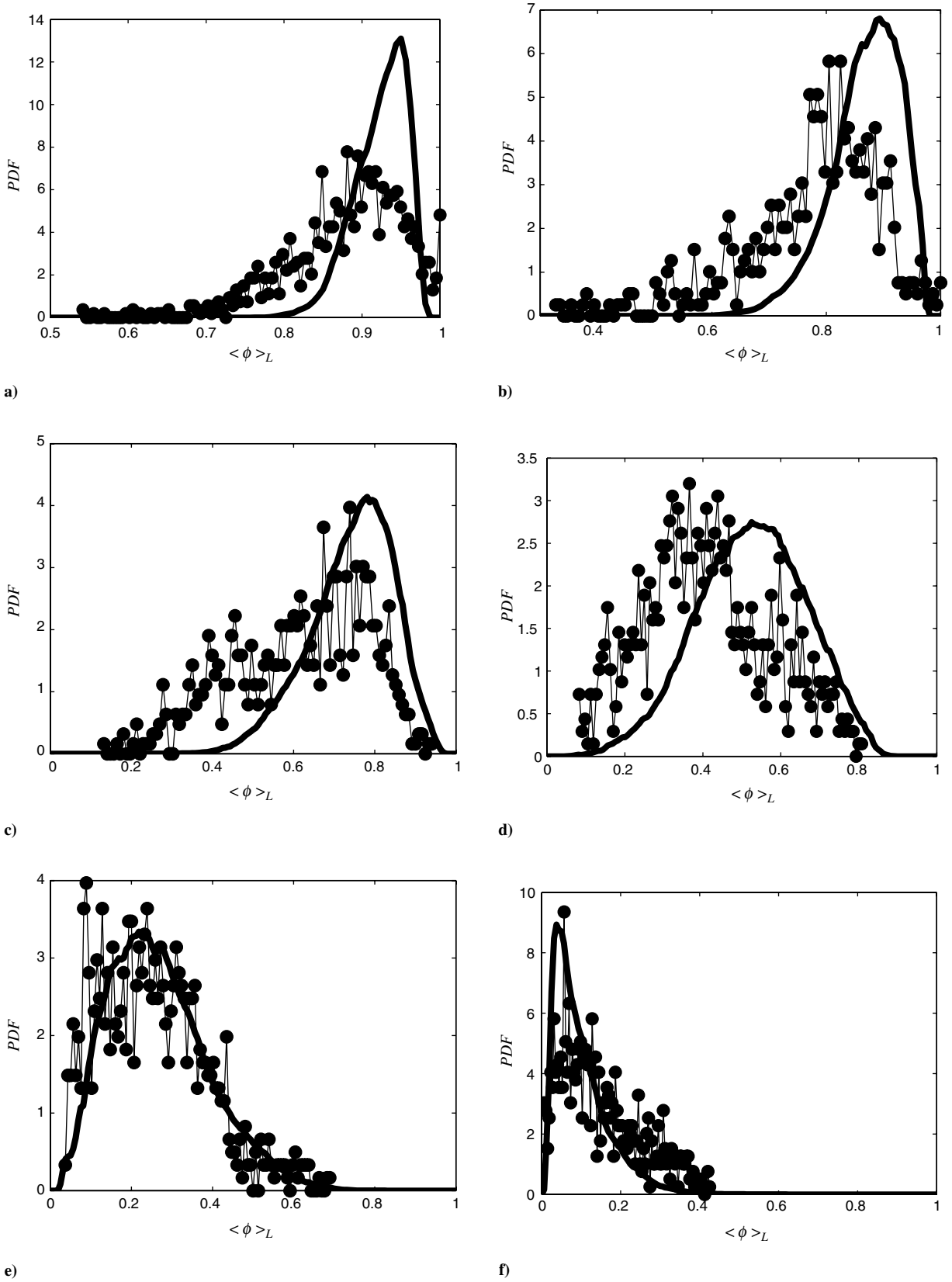

Fig. 12 PDF of the resolved filtered mixture fraction at $x/D = 15$ and different radial locations (from the centerline to the outer layer). The symbols and the thick lines denote the experimental data and LES predictions, respectively.

$16D \times 16D$ in the streamwise direction (x) and the two lateral directions (y and z). The number of grid points are $201 \times 161 \times 161$ in the x, y, and z directions, respectively. The filter size is set equal to $\Delta_L = 2(\Delta x \Delta y \Delta z)^{(1/3)}$, where Δx, Δy, and Δz denote the grid spacings in the corresponding directions. The MC particles are supplied in the inlet region and are free to move within the domain, due to combined actions of convection and diffusion. The volume of the ensemble domain is $\mathcal{V}_E = (\Delta x \Delta y \Delta z)$ within which $N_E \approx 40$; threfore, there are at least 200 million MC particles within the domain at all times.

The flow variables at the inflow are set the same as those in the experiments, including the inlet profiles of the velocity and the mixture fraction. The inlet condition for the velocity is presented in Fig. 1. The flow is excited by superimposing oscillating axisymmetric perturbations at the inflow. The procedure is similar to that in [45], but the amplitude of forcing is set in such a way to match the experimentally measured turbulent intensity of the streamwise velocity at the inlet. Standard characteristic boundary conditions [46] are implemented in all of the FD simulations.

The simulations' accuracy and the extent of resolved energy depend on the FD grid spacing, the volume of the ensemble domain, the number of MC particles, and the adopted values of the model constants. The effects of all of these parameters are investigated in [30]. Per the results of this study, the parameters as selected here yield an excellent statistical accuracy with minimal dispersion errors. Furthermore, the MC simulation results are monitored to ensure that the particles fully encompass and extend well beyond regions of nonzero vorticity and reaction.

The methane–air reaction mechanism, as occurs in this flame, is taken into account via the flamelet model. This model considers a laminar one-dimensional counterflow (opposed jet) flame configuration [47]. The detailed kinetics mechanism of the Gas Research Institute (GRI2.11) [48] is employed to describe combustion. The flamelet table at a strain rate of $a = 100$ 1/s is used to relate the thermochemical variables to the mixture fraction. This value is consistent with that used in previous SFMDF [12] and probability density function (PDF) [49] predictions of this flame. It also yields the best overall match of the one-dimensional results with experimental data. The predictive capability of VSFMDF is demonstrated by comparing the flow statistics with the Sandia–Darmstadt data [32,33]. These statistics are obtained by long time-averaging of the filtered field during six flow-through times. The notations $\bar{Q}$ and rms(Q) denote, respectively, the time-averaged mean and root-mean-square values of the variable Q. Simulations are conducted on 256 processors in conjunction with a message-passing interface and the PETSc [50–52] library.

IV. Results

For the purpose of flow visualization, the contour plots of FD and MC computations for normalized $\langle RT \rangle_L$ values are shown in Fig. 2. The central jet lies in the middle along the axial coordinate, surrounded by a pilot, where the temperature is the highest and encircled by the air coflow. The region close to inlet is dominated by the molecular diffusion and the jet exhibits a laminarlike behavior. Further downstream, the growth of perturbations is manifested by the formation of large-scale coherent vortices. The upstream feedback from the vortices created initially triggers further self-sustaining vortex rollup and subsequent pairing and coalescence of neighboring vortices [53,54]. The slight oscillations inherent in the FD simulations due to a fixed number of gird points are absent in the Lagrangian (grid-free) results. The streamwise variation of the time-averaged values of these results at the centerline is shown in Fig. 3, showing that the growth of the layer is predicted well.

The capability of the method in predicting the hydrodynamics field is demonstrated by examining some of the (reported) radial ($r = \sqrt{z^2 + y^2}$) distributions of the flow statistics in Fig. 4. The results at $x/D = 15$ are shown in this and all of the subsequent figures, as the profiles at other streamwise location portray similar behavior for the other statistical quantities considered. The VSFMDF predicts the peak value of mean axial velocity profile and the spread of the jet reasonably well. The rms values, however, are underpredicted. The radial distribution of the mixture fraction is also shown to compare well with data (Fig. 5). The mean and rms values are close to measured data.

The statistics of the thermochemical variables are also compared with corresponding data. The radial distribution of the mean temperature and its corresponding rms values are presented in Fig. 6. Similar to hydrodynamic quantities, the mean profiles show favorable agreement with measured data, whereas the rms values are underpredicted at the outer layer. The statistics of the mass fractions (denoted by Y) of several of the species at different streamwise locations are compared with data in Figs. 7–11. The mean profiles of the major species show close agreements with measurements. However, the mean values of the minor species are overpredicted. The rms values show close agreements with measured data at the inner layer, but not as good at the outer layer. These disagreements can be attributed, in part, to the shortcoming of the flamelet model in relating the thermochemical variables to the mixture fraction. In Fig. 12, the PDFs of the resolved mixture fraction as predicted by the VSFMDF are compared with those measured experimentally at several locations throughout the domain. In general, both the peak and the spreads of the PDFs are predicted well.

V. Conclusions

Since its original development a decade ago, the SFMDF [4,5] has experienced widespread applications for LES of a variety of reacting flows [6–8,10,11,13–26,29]. The methodology has found its way in industry [21] and is now covered as a powerful predictive tool in most modern textbooks and handbooks [34,47,55–58]. This popularity is partially due to the demonstrated capability of the method to simulate realistic hydrocarbon flame. The extended methodology, the VSFMDF, is significantly more powerful, as it also accounts for the effects of SGS convection in an exact manner. This superiority has been previously demonstrated by comparative assessment of the method in several basic flow configurations [30].

The objective of the present work is to assess the prospects of the VSFMDF for realistic flame simulations. For that, we consider a relatively simple flame: the piloted, nonpremixed, turbulent, methane jet flame (Sandia flame D). For this flame, which was previously simulated via SFMDF [12–14,19–24], the thermochemical variables are related to the mixture fraction via a flamelet table. A modeled transport equation for the mass-weighted joint FDF of the velocity and the mixture fraction [30] is considered. This equation is solved by a hybrid finite difference and Monte Carlo method. The predictive capability of the overall scheme is assessed by comparison of the ensemble (long time, Reynolds-averaged) values of the thermochemical variables. It is shown that all of the mean quantities are generally predicted well. For the rms values, the predicted values agree closely with the experimental data in the inner layer, but not as good in the outer layer. This discrepancy is attributed, in part, to the use of the flamelet model in relating all of the thermochemical variables to the mixture fraction. The PDFs of this mixture fraction as predicted by the model show very good agreements with data.

Some suggestions for future work are as follows:

1) Implement higher-order closures for the generalized Langevin model parameter G_{ij} [59]. The model parameters considered here correspond to Rotta's closure in RANS [34,60]. Higher-order closure similar to those considered in RANS [39,59] may be implemented.

2) Extend the methodology to account for differential diffusion effects [23,61–63]. The VSFMDF may be extended to flows with nonunity Prandtl and/or Schmidt numbers. It may also be extended to include temperature-dependent viscosity and diffusion coefficients.

3) Quantitatively assess data by performing simulations with different (combination) values for the grid spacings, filter sizes and the number of MC particles. Such assessments have been previously done in SFMDF [18], but require significant more computational resources for VSFMDF.

4) Extend the methodology for simulation of flames that experience extinction (such as Sandia flames E and F). Such simulations require consideration of finite rate chemistry.

Currently, it is not computationally feasible to implement detailed kinetics in VSFMDF or in SFMDF. Implementation of reduced-kinetics schemes is within reach, provided that sufficient computational resources are available.

Acknowledgments

This work is sponsored by NASA under grant NNX08AB36A and by the U.S. Air Force Office of Scientific Research with Julian M. Tishkoff as the Program Manager under grant FA9550-06-1-0015. The computations support is provided by the National Science Foundation through TeraGrid resources at the Pittsburgh Supercomputing Center.

References

[1] Pope, S. B., "Computations of Turbulent Combustion: Progress and Challenges," *Proceedings of the Combustion Institute*, Vol. 23, No. 1, 1990, pp. 591–612.

[2] Givi, P., "Model Free Simulations of Turbulent Reactive Flows," *Progress in Energy and Combustion Science*, Vol. 15, No. 1, 1989, pp. 1–107. doi:10.1016/0360-1285(89)90006-3

[3] Givi, P., "Filtered Density Function for Subgrid-Scale Modeling of Turbulent Combustion," *AIAA Journal*, Vol. 44, No. 1, 2006, pp. 16–23. doi:10.2514/1.15514

[4] Colucci, P. J., Jaberi, F. A., Givi, P., and Pope, S. B., "Filtered Density Function for Large Eddy Simulation of Turbulent Reacting Flows," *Physics of Fluids*, Vol. 10, No. 2, 1998, pp. 499–515. doi:10.1063/1.869537

[5] Jaberi, F. A., Colucci, P. J., James, S., Givi, P., and Pope, S. B., "Filtered Mass Density Function for Large Eddy Simulation of Turbulent Reacting Flows," *Journal of Fluid Mechanics*, Vol. 401, 1999, pp. 85–121. doi:10.1017/S0022112099006643

[6] Garrick, S. C., Jaberi, F. A., and Givi, P., "Large Eddy Simulation of Scalar Transport in a Turbulent Jet Flow," *Recent Advances in DNS and LES*, Vol. 54, edited by D. Knight, and L. Sakell, Kluwer Academic, Dordrecht, The Netherlands, 1999, pp. 155–166.

[7] James, S., and Jaberi, F. A., "Large Scale Simulations of Two-Dimensional Nonpremixed Methane Jet Flames," *Combustion and Flame*, Vol. 123, No. 4, 2000, pp. 465–487. doi:10.1016/S0010-2180(00)00178-4

[8] Zhou, X. Y., and Pereira, J. C. F., "Large Eddy Simulation (2D) of a Reacting Plan Mixing Layer Using Filtered Density Function," *Flow, Turbulence and Combustion*, Vol. 64, No. 4, 2000, pp. 279–300. doi:10.1023/A:1026595626129

[9] Zhou, X., and Mahalingam, S., "A Flame Surface Density Based Model for Large Eddy Simulation of Turbulent Nonpremixed Combustion," *Physics of Fluids*, Vol. 14, No. 11, 2002, pp. 77–80. doi:10.1063/1.1518691

[10] Heinz, S., "On Fokker-Planck Equations for Turbulent Reacting Flows. Part 2. Filter Density Function for Large Eddy Simulation, *Flow, Turbulence and Combustion*, Vol. 70, Nos. 1–4, 2003, pp. 153–181. doi:10.1023/B:APPL.0000004934.22265.74

[11] Cha, C. M., and Troullet, P., "A Subgrid-Scale Mixing Model for Large-Eddy Simulations of Turbulent Reacting Flows Using the Filtered Density Function," *Physics of Fluids*, Vol. 15, No. 6, 2003, pp. 1496–1504. doi:10.1063/1.1569920

[12] Sheikhi, M. R. H., Drozda, T. G., Givi, P., Jaberi, F. A., and Pope, S. B., "Large Eddy Simulation of a Turbulent Nonpremixed Piloted Methane Jet Flame (Sandia Flame D)," *Proceedings of the Combustion Institute*, Vol. 30, No. 1, 2005, pp. 549–556. doi:10.1016/j.proci.2004.08.028

[13] Raman, V., Pitsch, H., and Fox, R. O., "Hybrid Large-Eddy Simulation/Lagrangian Filtered Density Function Approach for Simulating Turbulent Combustion," *Combustion and Flame*, Vol. 143, Nos. 1–2, 2005, pp. 56–78. doi:10.1016/j.combustflame.2005.05.002

[14] Raman, V., and Pitsch, H., "Large-Eddy Simulation of a Bluff-Body-Stabilized Nonpremixed Flame Using a Recursive Filter-Refinement Procedure," *Combustion and Flame*, Vol. 142, No. 4, 2005, pp. 329–347. doi:10.1016/j.combustflame.2005.03.014

[15] van Vliet, E., Derksen, J. J., and van den Akker, H. E. A., "Turbulent Mixing in a Tubular Reactor: Assessment of an FDF/LES Approach," *AIChE Journal*, Vol. 51, No. 3, 2005, pp. 725–739. doi:10.1002/aic.10365

[16] Carrara, M. D., and DesJardin, P. E., "A Filtered Mass Density Function Approach to Modeling Separated Two-Phase Flows Using LES I: Mathematical Formulation," *International Journal of Multiphase Flow*, Vol. 32, No. 3, 2006, pp. 365–384. doi:10.1016/j.ijmultiphaseflow.2005.11.003

[17] Mustata, R., Valĩno, L., Jiménez, C., Jones, W. P., and Bondi, S., "A Probability Density Function Eulerian Monte Carlo Field Method for Large Eddy Simulations: Application to a Turbulent Piloted Methane/Air Diffusion Flame (Sandia d)," *Combustion and Flame*, Vol. 145, Nos. 1–2, 2006, pp. 88–104. doi:10.1016/j.combustflame.2005.12.002

[18] Drozda, T. G., Sheikhi, M. R. H., Madnia, C. K., and Givi, P., "Developments in Formulation and Application of the Filtered Density Function," *Flow, Turbulence and Combustion*, Vol. 78, No. 1, 2007, pp. 35–67.

[19] Jones, W. P., Navarro-Martinez, S., and Röhl, O., "Large Eddy Simulation of Hydrogen Auto-Ignition with a Probability Density Function Method," *Proceedings of the Combustion Institute*, Vol. 31, No. 2, 2007, pp. 1765–1771. doi:10.1016/j.proci.2006.07.041

[20] Jones, W. P., and Navarro-Martinez, S., "Large Eddy Simulation of Autoignition with a Subgrid Probability Density Function Method," *Combustion and Flame*, Vol. 150, No. 3, 2007, pp. 170–187. doi:10.1016/j.combustflame.2007.04.003

[21] James, S., Zhu, J., and Anand, M. S., "Large Eddy Simulations of Turbulent Flames Using the Filtered Density Function Model," *Proceedings of the Combustion Institute*, Vol. 31, No. 2, 2007, pp. 1737–1745. doi:10.1016/j.proci.2006.07.160

[22] Chen, J. Y., "A Eulerian PDF Scheme for LES of Nonpremixed Turbulent Combustion with Second-Order-Accurate Mixture Fraction," *Combustion Theory and Modelling*, Vol. 11, No. 5, 2007, pp. 675–695. doi:10.1080/13647830601091723

[23] McDermott, R., and Pope, S. B., "A Particle Formulation for Treating Differential Diffusion in Filtered Density Function Methods," *Journal of Computational Physics*, Vol. 226, No. 1, 2007, pp. 947–993. doi:10.1016/j.jcp.2007.05.006

[24] Raman, V., and Pitsch, H., "A Consistent LES/Filtered-Density Function Formulation for the Simulation of Turbulent Flames with Detailed Chemistry," *Proceedings of the Combustion Institute*, Vol. 31, No. 2, 2007, pp. 1711–1719. doi:10.1016/j.proci.2006.07.152

[25] Afshari, A., Jaberi, F. A., and Shih, T.I. P., "Large-Eddy Simulations of Turbulent Flows in an Axisymmetric Dump Combustor," *AIAA Journal*, Vol. 46, No. 7, 2008, pp. 1576–1592. doi:10.2514/1.25467

[26] Drozda, T. G., Wang, G., Sankaran, V., Mayo, J. R., Oefelein, J. C., and Barlow, R. S., "Scalar Filtered Mass Density Functions in Nonpremixed Turbulent Jet Flames," *Combustion and Flame*, Vol. 155, Nos. 1–2, 2008, pp. 54–69. doi:10.1016/j.combustflame.2008.06.012

[27] Givi, P., Sheikhi, M. R. H., Drozda, T. G., and Madnia, C. K., "Large Scale Simulation of Turbulent Combustion," *Combust. Plasma Chem.*, Vol. 6, No. 1, 2008, pp. 1–9.

[28] Gicquel, L. Y. M., Givi, P., Jaberi, F. A., and Pope, S. B., "Velocity Filtered Density Function for Large Eddy Simulation of Turbulent Flows," *Physics of Fluids*, Vol. 14, No. 3, 2002, pp. 1196–1213. doi:10.1063/1.1436496

[29] Sheikhi, M. R. H., Drozda, T. G., Givi, P., and Pope, S. B., "Velocity-Scalar Filtered Density Function for Large Eddy Simulation of Turbulent Flows," *Physics of Fluids*, Vol. 15, No. 8, 2003, pp. 2321–2337. doi:10.1063/1.1584678

[30] Sheikhi, M. R. H., Givi, P., and Pope, S. B., "Velocity-Scalar Filtered Mass Density Function for Large Eddy Simulation of Turbulent Reacting Flows," *Physics of Fluids*, Vol. 19, No. 9, 2007, Paper 095106. doi:10.1063/1.2768953

[31] Sagaut, P., *Large Eddy Simulation for Incompressible Flows*, 3rd ed., Springer–Verlag, New York, 2005.

[32] Nooren, P. A., Versiuis, M., Van der Meer, T. H., Barlow, R. S., and Frank, J. H., "Raman-Rayleigh-LIF Measurements of Temperature and Species Concentrations in the Delft Piloted Turbulent Jet Diffusion Flame," *Applied Physics B (Lasers and Optics)*, Vol. 71, No. 1, 2000, pp. 95–111. doi:10.1007/s003400000278

[33] Schneider, C., Dreizler, A., Janicka, J., and Hassel, E. P., "Flow Field

Measurements of Stable and Locally Extinguishing Hydrocarbonfuelled Jet Flames, *Combustion and Flame*, Vol. 135, No. 1, 2003, pp. 185–190. doi:10.1016/S0010-2180(03)00150-0

[34] Pope, S. B., *Turbulent Flows*, Cambridge Univ. Press, Cambridge, England, U.K., 2000.

[35] O'Brien, E. E., "The Probability Density Function (PDF) Approach to Reacting Turbulent Flows," edited by P. A. Libby, and F. A. Williams, *Turbulent Reacting Flows*, Vol. 44, Springer–Verlag, Heidelberg, 1980, Chap. 5, pp. 185–218.

[36] Pope, S. B., "PDF Methods for Turbulent Reactive Flows," *Progress in Energy and Combustion Science*, Vol. 11, No. 2, 1985, pp. 119–192. doi:10.1016/0360-1285(85)90002-4

[37] Vreman, B., Geurts, B., and Kuerten, H., "Realizability Conditions for the Turbulent Stress Tensor in Large-Eddy Simulation," *Journal of Fluid Mechanics*, Vol. 278, 1994, pp. 351–362. doi:10.1017/S0022112094003745

[38] Karlin, S., and Taylor, H. M., *A Second Course in Stochastic Processes*, Academic Press, New York, 1981.

[39] Haworth, D. C., and Pope, S. B., "A Generalized Langevin Model for Turbulent Flows," *Physics of Fluids*, Vol. 29, No. 2, 1986, pp. 387–405. doi:10.1063/1.865723

[40] Dreeben, T. D., and Pope, S. B., "Probability Density Function and Reynolds-Stress Modeling of Near-Wall Turbulent Flows," *Physics of Fluids*, Vol. 9, No. 1, 1997, pp. 154–163. doi:10.1063/1.869157

[41] Wax, N., *Selected Papers on Noise and Stochastic Processes*, Dover, New York, 1954.

[42] Gardiner, C. W., *Handbook of Stochastic Methods*, Springer–Verlag, New York, 1990.

[43] Madnia, C. K., Jaberi, F. A., and Givi, P., "Large Eddy Simulation of Heat and Mass Transport in Turbulent Flows," *Handbook of Numerical Heat Transfer*, 2nd. ed., Wiley, New York, 2006, Ch. 5, pp. 167–189.

[44] Kennedy, C. A., and Carpenter, M. H., "Several New Numerical Methods for Compressible Shear-Layer Simulations," *Applied Numerical Mathematics*, Vol. 14, No. 4, 1994, pp. 397–433. doi:10.1016/0168-9274(94)00004-2

[45] Danaila, I., and Boersma, B. J., "Direct Numerical Simulation of Bifurcating Jets," *Physics of Fluids*, Vol. 12, No. 5, 2000, pp. 1255–1257. doi:10.1063/1.870377

[46] Poinsot, T. J., and Lele, S. K., "Boundary Conditions for Direct Simulations of Compressible Viscous Flows," *Journal of Computational Physics*, Vol. 101, No. 1, 1992, pp. 104–129. doi:10.1016/0021-9991(92)90046-2

[47] Peters, N., *Turbulent Combustion*, Cambridge Univ. Press, Cambridge, England, U.K., 2000.

[48] GRI-Mech, Software Package, Ver. 3.0, http://www.me.berkeley.edu/gri_mech, Gas Research Inst., Chicago, IL.

[49] Muradoglu, M., Liu, K., and Pope, S. B., "PDF Modeling of a Bluff-Body Stabilized Turbulent Flame," *Combustion and Flame*, Vol. 132, Nos. 1–2, 2003, pp. 115–137. doi:10.1016/S0010-2180(02)00430-3

[50] PETSc: Portable, Extensible Toolkit for Scientific Computation, Software Package, Ver. 3.0.0, MSD Div., Argonne National Lab., Argonne, IL, 2008, http://www.mcs.anl.gov/petsc [retrieved 8 March 2010].

[51] *PETSc Users Manual*, Argonne National Lab., TR ANL-95/11, Rev. 2.1.5, Argonne, IL, 2004.

[52] Balay, S., Gropp, W. D., McInnes, L. C., and Smith, B. F., "Efficient Management of Parallelism in Object Oriented Numerical Software Libraries, *Modern Software Tools in Scientific Computing*, edited by E. Arge, A. M. Bruaset, and H. P. Langtangen, Birkhäuser, Boston, 1997, pp. 163–202.

[53] Givi, P., and Riley, J. J., "Some Current Issues in the Analysis of Reacting Shear Layers: Computational Challenges," *Major Research Topics in Combustion*, edited by M. Y. Hussaini, A. Kumar, and R. G. Voigt, Springer–Verlag, New York, 1992, pp. 588–650.

[54] Drummond, J. P., and Givi, P., "Suppression and Enhancement of Mixing in High-Speed Reacting Flow Fields," *Combustion in High-Speed Flows*, edited by J. D. Buckmaster, T. L. Jackson, and A. Kumar, Kluwer Academic, Dordrecht, The Netherlands, 1994, pp. 191–229.

[55] Bilger, R. W., "Future Progress in Turbulent Combustion Research," *Progress in Energy and Combustion Science*, Vol. 26, Nos. 4–6, 2000, pp. 367–380. doi:10.1016/S0360-1285(00)00015-0

[56] Fox, R. O., *Computational Models for Turbulent Reacting Flows*, Cambridge Univ. Press, Cambridge, England, U.K., 2003.

[57] Heinz, S., "On Fokker-Planck Equations for Turbulent Reacting Flows. Part 2. Filtered Density Function for Large Eddy Simulation," *Flow, Turbulence and Combustion*, Vol. 70, Nos. 1–4, 2003, pp. 153–181. doi:10.1023/B:APPL.0000004934.22265.74

[58] Minkowycz, W. J., Sparrow, E. M., and J. Y. Murthy, *Handbook of Numerical Heat Transfer*, 2nd ed., Wiley, New York, 2006.

[59] Pope, S. B., "On the Relation Between Stochastic Lagrangian Models of Turbulence and Second-Moment Closures," *Physics of Fluids*, Vol. 6, No. 2, 1994, pp. 973–985. doi:10.1063/1.868329

[60] Wilcox, D. C., *Turbulence Modeling for CFD*, DCW Industries, La Cãnada, CA, 1993.

[61] Jaberi, F. A., Miller, R. S., Mashayek, F., and Givi, P., "Differential Diffusion in Binary Scalar Mixing and Reaction," *Combustion and Flame*, Vol. 109, No. 4, 1997, pp. 561–577. doi:10.1016/S0010-2180(97)00045-X

[62] Kerstein, A. R., Cremer, M. A., and McMurtry, P. A., "Scaling Properties of Differential Molecular Diffusion Effects in Turbulence," *Physics of Fluids*, Vol. 7, No. 8, 1995, pp. 1999–2007. doi:10.1063/1.868511

[63] Yeunga, P. K., Xu, S., and Sreenivasan, K. R., "Schmidt Number Effects on Turbulent Transport with Uniform Mean Scalar Gradient," *Physics of Fluids*, Vol. 14, No. 12, 2002, pp. 4178–4191. doi:10.1063/1.1517298

T. Jackson
Associate Editor